

On the next-to-leading order QCD \mathcal{K} -factor for $t\bar{t}b\bar{b}$ production at the TeVatron

Małgorzata Worek^a

^a*Fachbereich C, Bergische Universität Wuppertal, D-42097 Wuppertal, Germany*

E-mail: worek@physik.uni-wuppertal.de

ABSTRACT: Motivated by ongoing experimental analyses, we report on the calculation of next-to-leading order QCD corrections to the production of $t\bar{t}$ pairs in association with two hard b-jets at the Fermilab TeVatron. Besides the total cross section and its scale dependence, a few differential distributions applicable for Higgs boson searches at the TeVatron are given. The QCD corrections with respect to leading order are negative and small. For our main setup they amount to 2%, and remain reasonably stable against changes of cuts. This proves that an integrated next-to-leading order \mathcal{K} -factor does not necessarily need to be applied in the background estimation for the $t\bar{t}H \rightarrow t\bar{t}b\bar{b}$ signal process. The distributions show similarly small corrections. The shape of kinematic distributions is distorted at most by about 20% in some corners of the phase space. Even though it is not the main purpose of this paper, we also evaluated the forward-backward asymmetry of the top quark at next-to-leading order.

KEYWORDS: NLO Computations, QCD, Higgs Physics, Standard Model

WUB/11-25

Contents

1	Introduction	1
2	Theoretical Framework	2
3	Phenomenological Results	2
3.1	Integrated Cross Sections	4
3.2	Differential Cross Sections	6
3.3	Forward-Backward Asymmetry	8
4	Summary and Conclusions	10

1 Introduction

The production of the Standard Model Higgs boson in association with a top-anti-top pair allows for a direct study of the top Yukawa coupling, which is an important step in understanding the nature of the electroweak symmetry breaking mechanism. The $t\bar{t}H$ production channel is especially important in the range of Higgs boson masses $m_H \leq 140$ GeV, where the Higgs boson decays predominantly into $b\bar{b}$ pairs. While the LHC is making ground breaking progress towards discovering the Higgs boson, and certainly tightens exclusion bounds well past those obtained at the TeVatron, the analysis of the data from the latter is still being completed. It is a fact that the predicted cross section for Higgs boson radiation off top quarks at the TeVatron is rather low [1–4]. Therefore, a discovery of the Higgs boson in this channel alone would not have been possible. However, it contributes to the combination of the Standard Model Higgs boson searches [5]. The main background process consists of direct production of the final state without resonances, i.e. of the QCD generated process $t\bar{t}b\bar{b}$. The procedure used by the experimental collaborations for the background estimate, is either direct use of leading order (LO) Monte Carlo simulations [6], or additional reweighting by a K-factor [7]. Unfortunately, a next-to-leading order (NLO) K-factor for this process under TeVatron conditions has never been published. According to [7], the analysis employs the published value [8] for the LHC. Since the production mechanisms are very different in both cases, it is questionable that such a procedure leads to reliable estimates. In this paper, we address this issue by providing an NLO QCD prediction to $t\bar{t}b\bar{b}$, the irreducible QCD background to the $t\bar{t}H \rightarrow t\bar{t}b\bar{b}$ process at the TeVatron.

2 Theoretical Framework

At tree level, $t\bar{t}$ production in association with two b-jets proceeds via the scattering of two gluons or two quarks. A few examples of LO graphs contributing to $p\bar{p} \rightarrow t\bar{t}b\bar{b}$ production are shown in Figure 1. The virtual corrections are obtained from the interference of the sum of all one-loop diagrams with the Born amplitude. One can classify them into self-energy, vertex, box-type, pentagon-type and hexagon-type corrections. In Figure 2 a few examples of pentagon and hexagon diagrams contributing to the virtual corrections to the $p\bar{p} \rightarrow t\bar{t}b\bar{b}$ process are given. And finally, the real emission corrections to the LO process arise from tree level amplitudes with one additional parton, an additional gluon, or a quark anti-quark pair replacing a gluon. All possible contributions can be divided into four subprocesses, $q\bar{q} \rightarrow t\bar{t}b\bar{b}g$, $gg \rightarrow t\bar{t}b\bar{b}g$, $qg \rightarrow t\bar{t}b\bar{b}q$ and $gq \rightarrow t\bar{t}b\bar{b}q$. In Figure 3 a representative set of Feynman diagrams contributing to the real emission corrections is shown.

The calculation of NLO corrections to $p\bar{p} \rightarrow t\bar{t}b\bar{b}$ production proceeds along the same lines as our earlier work on $pp \rightarrow t\bar{t}b\bar{b}$ [8], $pp(p\bar{p}) \rightarrow t\bar{t}jj$ [9, 10] and $pp(p\bar{p}) \rightarrow W^+W^-b\bar{b} \rightarrow e^+\nu_e\mu^-\bar{\nu}_\mu b\bar{b}$ [11]. The methods and internal tests developed there have therefore been straightforwardly adapted for this project. Let us stress here, that results for the $pp \rightarrow t\bar{t}b\bar{b}$ and $pp(p\bar{p}) \rightarrow W^+W^-b\bar{b}$ processes have also been obtained by other groups [12–14].

To summarize briefly, off-shell methods and the OPP reduction procedure [15], as implemented in the HELAC-NLO system [16] are used in computing the NLO QCD corrections for the $p\bar{p} \rightarrow t\bar{t}b\bar{b}$ processes. The system consists of, CUTTOOLS [17–20] and HELAC-1LOOP [21], which handle the virtual corrections and HELAC-DIPOLES [22] for the real emission contributions. For the phase space integration, the KALEU package [23] is used and results are cross checked with the help of the PHEGAS phase space generator [24]. Moreover, ONELOOP [25] is employed for the evaluation of the one-loop scalar functions.

LO results, which are generated with HELAC-DIPOLES have been cross checked with HELAC-PHEGAS¹ [26–28]. Perfect agreement has been found. The numerical stability of virtual corrections has been monitored by checking Ward identities at every phase space point. Those events, which violate gauge invariance (0.13% out of all 2×10^5 generated unweighted events for which one-loop contributions are calculated) have been recalculated with quadruple precision. In addition, the cancellation of soft and collinear divergences after combining virtual and real corrections has been checked numerically for a few phase space points.

3 Phenomenological Results

In the following, we present predictions for the $t\bar{t}b\bar{b} + X$ process at the TeVatron run II with $\sqrt{s} = 1.96$ TeV. We use the Tevatron average mass of the top quark $m_t = 173.3$ GeV as measured by the CDF and D0 experiments [34]. The masses of all other quarks, including b quarks, are neglected. We have consistently employed the MSTW2008 set of parton distribution functions (PDFs) [35]. In particular, we take MSTW2008LO PDFs with 1-loop running α_s at LO and MSTW2008NLO PDFs with 2-loop running α_s at NLO, including

¹Let us stress that HELAC-PHEGAS has already been extensively used and tested, see e.g. [29–33].

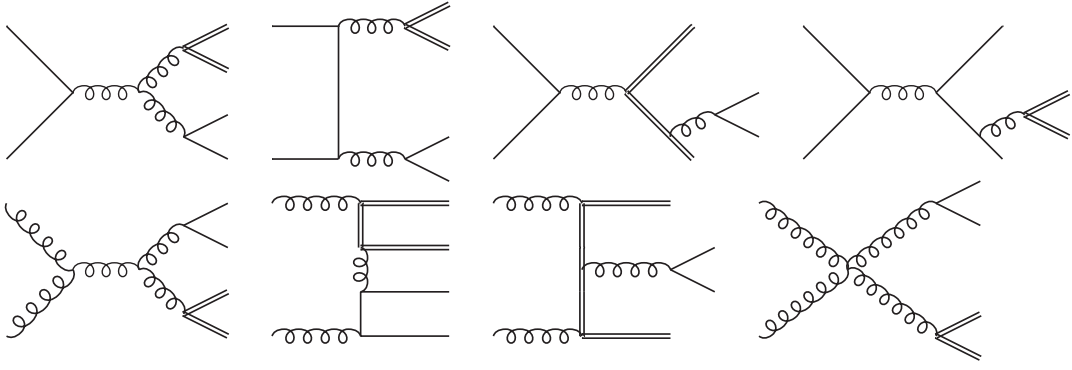


Figure 1. A representative set of Feynman diagrams contributing to the leading order $p\bar{p} \rightarrow t\bar{t}b\bar{b}$ process. Double lines correspond to top quarks, single lines to light quarks and wiggly ones to gluons.

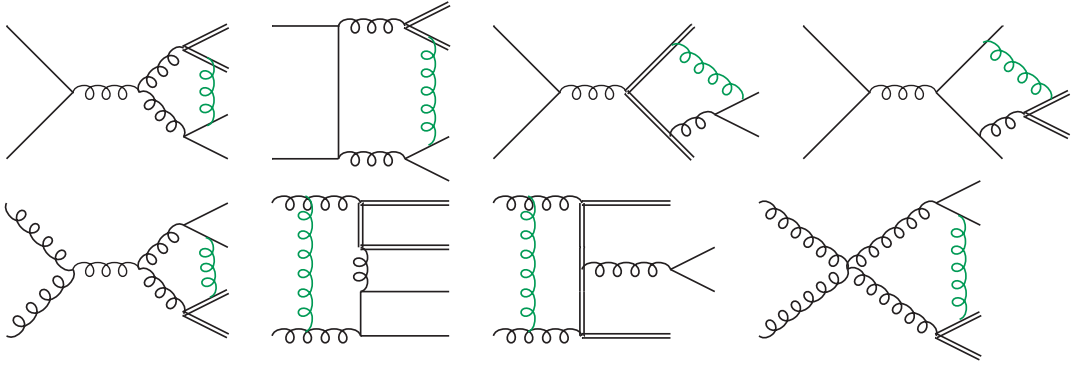


Figure 2. A representative set of pentagon and hexagon diagrams contributing to the virtual corrections to the $p\bar{p} \rightarrow t\bar{t}b\bar{b}$ process. Double lines correspond to top quarks, single lines to light quarks and wiggly ones to gluons.

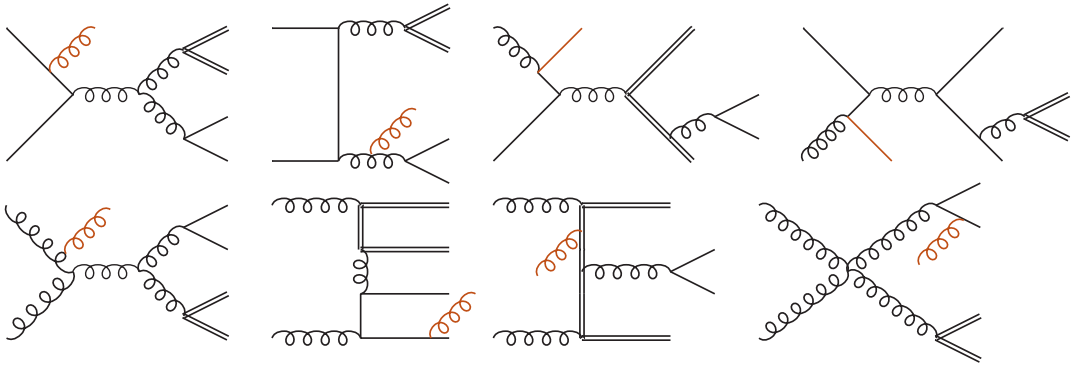


Figure 3. A representative set of Feynman diagrams contributing to the real emission corrections to the $p\bar{p} \rightarrow t\bar{t}b\bar{b}$ process. Double lines correspond to top quarks, single lines to light quarks and wiggly ones to gluons.

five active flavors. Contributions induced by bottom-quark densities are not taken into account due to their negligible size. The renormalization and factorization scales are set to a common value $\mu_R = \mu_F = \mu = m_t$. All final-state massless partons with pseudorapidity $|\eta| < 5$, defined as $\eta = -\ln[\tan(\theta/2)]$, where θ is the angle between the parton momentum and the beam axis, are recombined into jets with a resolution parameter $R = 0.8$ via an IR-safe algorithm. We have applied three different jets algorithms: k_T [36–38], *anti- k_T* [39] and the Cambridge/Aachen (C/A) algorithm [40]. For our main setup, two b-jets are required to have

$$p_T(b) > 20 \text{ GeV}, \quad |y(b)| < 2.5, \quad \Delta R_{b\bar{b}} > 0.8, \quad (3.1)$$

where $p_T(b)$, $y(b)$ are the transverse momentum and rapidity of the b-jet, and $\Delta R_{b\bar{b}}$ is the separation in the plane of rapidity and azimuthal angle between $b\bar{b}$ pairs. Jets momenta are formed as the four-vector sum of massless parton momenta. At LO, there are exactly two massless final state partons, which are identified as two b-jets, provided they pass the cuts described above. At NLO, a third parton might emerge. It could be recombined with another parton to give a b-jet, or an additional jet with unrestricted kinematics may appear. Outgoing top and anti-top quarks are left on-shell, they do not undergo any cut selection.

3.1 Integrated Cross Sections

We start with the total cross sections. In Table 1 and Table 2 integrated cross sections at LO and NLO for $p\bar{p} \rightarrow t\bar{t}b\bar{b} + X$ production at the TeVatron run II are presented. In Table 2, the scale dependence of the total cross section is also given. Using a fixed scale independent of the final state kinematics, which we set to m_t and estimate the error with the usual variation in the range between $m_t/2$ and $2m_t$ our findings can be summarized as follows

$$\sigma_{\text{LO}}(\text{TeVATRON}, m_t = 173.3 \text{ GeV}, \text{MSTW2008LO}) = 3.912^{+3.496(89\%)}_{-1.705(43\%)} \text{ fb}, \quad (3.2)$$

$$\sigma_{\text{NLO}}(\text{TeVATRON}, m_t = 173.3 \text{ GeV}, \text{MSTW2008NLO}) = 3.835^{+0.992(26\%)}_{-1.015(26\%)} \text{ fb}, \quad (3.3)$$

which leaves us with an NLO \mathcal{K} -factor equal to $\mathcal{K} = 0.98$ and a negative NLO QCD correction of the order of 2%. This is very different from the LHC case, where the same cut selection implies NLO corrections of the order of 77% [8, 12]. There, a dynamical scale, $\mu = m_t \sqrt{p_T(b)p_T(\bar{b})}$, and $m_{b\bar{b}} \geq 100 \text{ GeV}$ had to be introduced in order to reduce the high corrections down to 25% – 30% [13]. The dissimilarity between the size of NLO QCD corrections comes mostly from the difference in the production process. At the TeVatron, with our cut selection the $q\bar{q}$ channel dominates the total LO $p\bar{p}$ cross section at about 91% followed by the gg channel with about 9%. In contrast, the gg channel comprises about 94% of the LO pp cross section at the LHC, followed by the $q\bar{q}$ channel with about 6%.

To assess the effect of changing the jet algorithm, we compare NLO results for different jet finders, the k_T , *anti- k_T* and the inclusive Cambridge/Aachen (C/A) jet algorithms as shown in Table 1. No significant change of the results due to the choice of the jet algorithm is observed. Differences are below 1%.

In Equation (3.2) and Equation (3.3) the scale dependence is indicated by the upper and lower values. The upper (lower) value represents the change when the scale is shifted towards $\mu = m_t/2$ ($\mu = 2m_t$). Rescaling the common scale from the default value m_t up and down by a factor 2 changes the cross section at LO by 89%. On the other hand, the improvement in the scale stability at NLO is prominent. The scale uncertainty is reduced down to 26%.

	σ_{LO} [fb]	$\sigma_{\text{NLO}}^{\text{anti-k}_T}$ [fb]	$\sigma_{\text{NLO}}^{\text{k}_T}$ [fb]	$\sigma_{\text{NLO}}^{\text{C/A}}$ [fb]
$\alpha_{\text{max}} = 1$	3.912(3)	3.835(3)	3.859(3)	3.853(3)
$\alpha_{\text{max}} = 0.01$	3.912(3)	3.836(5)	3.861(5)	3.856(5)

Table 1. Integrated cross section at LO and NLO for $p\bar{p} \rightarrow t\bar{t}b\bar{b} + X$ production at the TeVatron run II. Results for three different jet algorithms and two different values of α_{max} are presented. The scale choice is $\mu = m_t$.

	$0.5 \cdot m_t$	$1 \cdot m_t$	$2 \cdot m_t$
σ_{LO} [fb]	7.408(5)	3.912(3)	2.207(2)
σ_{NLO} [fb]	4.827(8)	3.835(3)	2.820(3)

Table 2. Scale dependence of the total cross section for $p\bar{p} \rightarrow t\bar{t}b\bar{b} + X$ production at the TeVatron run II at LO and NLO with $\mu = \xi \cdot m_t$.

In addition, integrated NLO cross sections for two values of the unphysical cutoff parameter α_{max} , which is a common modification of subtraction terms in the phase space away from the singularity first introduced in [41], are given in Table 1. To be specific, $\alpha_{\text{max}} = 1$, which corresponds to the original formulation of [42, 43], and $\alpha_{\text{max}} = 0.01$ are considered. The independence of the final result on the value of the α_{max} parameter is obtained at the per-mil level. This is a strong consistency check of the calculation of the real emission part. For more details on the α_{max} implementation in the HELAC-DIPOLES package see e.g. [8, 22].

Results for a slightly modified setup have also been generated, to determine the stability of the NLO \mathcal{K} -factor. On the one hand, a higher transverse momentum cut on the b-jet of 40 GeV has been chosen. On the other hand, a higher jet separation cut, $\Delta R_{b\bar{b}} > 1$ has been used together with a new jet resolution parameter $R = 1$. All other parameters have been left unchanged. With this modified selection of cuts the integrated NLO \mathcal{K} -factor has changed from 0.98 to 0.88. More precisely, we have obtained the following integrated cross section at LO and NLO

$$\sigma_{\text{LO}} = 0.8135(6) \text{ fb}, \quad (3.4)$$

$$\sigma_{\text{NLO}} = 0.7121(10) \text{ fb}, \quad (3.5)$$

which results in negative NLO QCD corrections of the order of 12%.

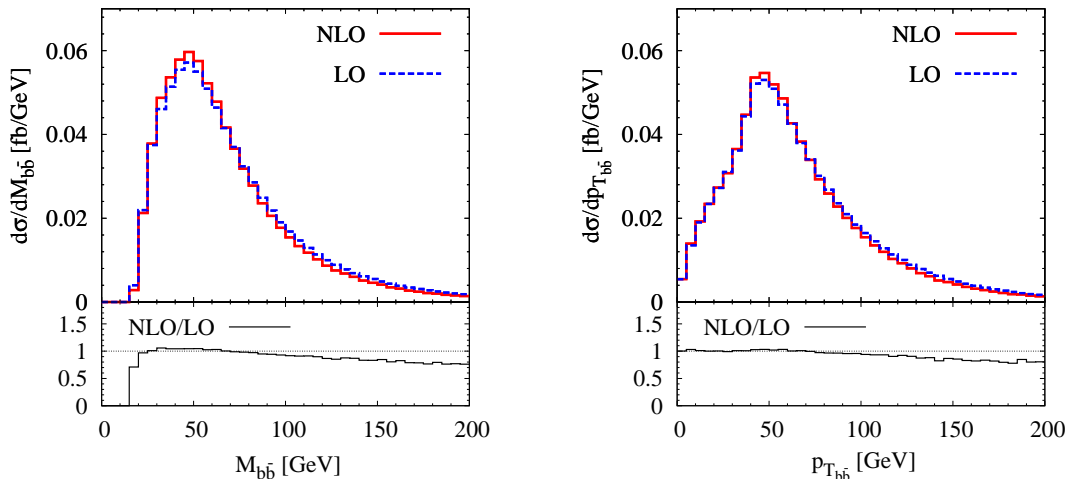


Figure 4. Distribution of the invariant mass $m_{b\bar{b}}$ (left panel) and distribution in the transverse momentum $p_{T_{b\bar{b}}}$ (right panel) of the bottom-anti-bottom pair for $p\bar{p} \rightarrow t\bar{t}b\bar{b} + X$ at the TeVatron run II at LO (blue dashed line) and NLO (red solid line). The lower panels display the differential K factor.

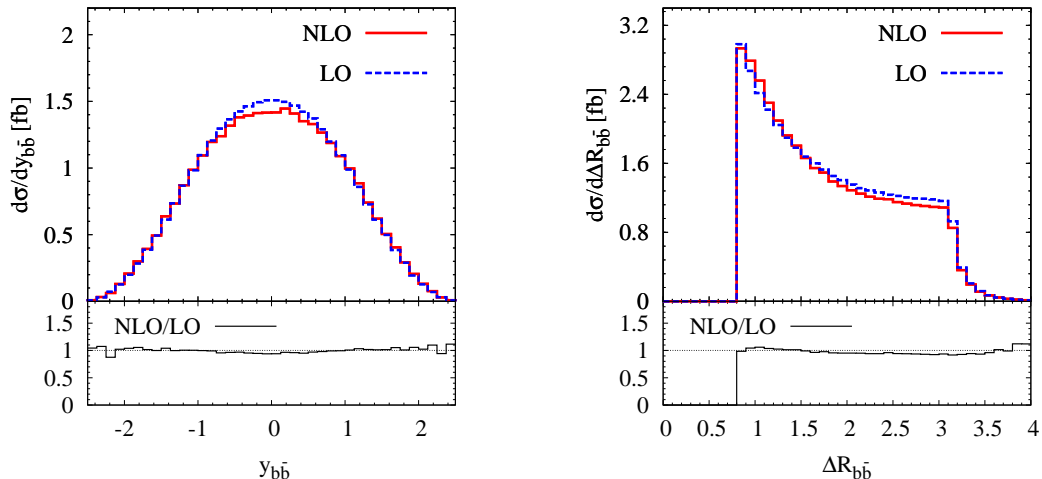


Figure 5. Distribution in the rapidity $y_{b\bar{b}}$ (left panel) of the bottom-anti-bottom pair and distribution of the $\Delta R_{b\bar{b}}$ separation (right panel) for $p\bar{p} \rightarrow t\bar{t}b\bar{b} + X$ at the TeVatron run II at LO (blue dashed line) and NLO (red solid line). The lower panels display the differential K factor.

3.2 Differential Cross Sections

In the following, the impact of QCD corrections on differential cross sections is analyzed. The differential distributions relevant for Higgs boson searches in the $t\bar{t}H \rightarrow t\bar{t}b\bar{b}$ channel are plotted first. In Figure 4, the distribution of the invariant mass $m_{b\bar{b}}$ and the distribution in the transverse momentum $p_{T_{b\bar{b}}}$ of the bottom-anti-bottom pair for $p\bar{p} \rightarrow t\bar{t}b\bar{b} + X$ at the TeVatron run II is plotted. The dashed curve corresponds to the LO, whereas the solid one

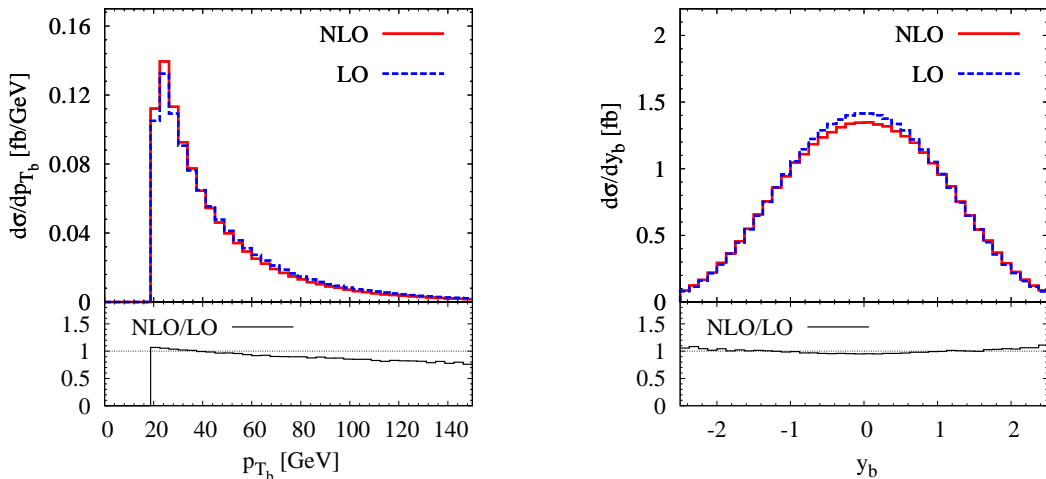


Figure 6. Distribution in the transverse momentum p_{T_b} (left panel) and distribution in the rapidity y_b (right panel) of the bottom quark for $p\bar{p} \rightarrow t\bar{t}b\bar{b} + X$ at the TeVatron run II at LO (blue dashed line) and NLO (red solid line). The lower panels display the differential \mathcal{K} factor.

to the NLO result. The upper panels show the distributions themselves while the lower panels display the ratio of the NLO value to the LO result, calculated according to

$$\mathcal{K}(\mathcal{O}) = \frac{d\sigma_{\text{NLO}}/d\mathcal{O}}{d\sigma_{\text{LO}}/d\mathcal{O}}, \quad (3.6)$$

for an observable \mathcal{O} under investigation, called the differential or dynamical \mathcal{K} factor. In Figure 5, the distribution in the rapidity $y_{b\bar{b}}$ of the bottom-anti-bottom pair and the distribution of the $\Delta R_{b\bar{b}}$ separation between two b-jets are shown. In all cases, the small NLO corrections of the integrated cross section are also visible at the differential level. In case of the most important observable, the $m_{b\bar{b}}$ differential distribution, in the phenomenologically relevant region, i.e. below 140 GeV, corrections of the order of $\sim 10\%$ are reached. Besides, the separation between the b-jets of 0.8 together with the transverse momentum cut on b-jets of 20 GeV sets an effective lower bound on the invariant mass of two b-jets of the order of $m_{b\bar{b}} \gtrsim 15.6$ GeV [8]. If we had chosen $\Delta R_{b\bar{b}} \geq 0.5$ the minimum $m_{b\bar{b}}$ would have been around 9.9 GeV instead.

In view of the small NLO corrections to the total cross sections as well as to the differential distributions presented here, we conclude that a meaningful analysis at the TeVatron can be performed with the present setup, i.e. with the renormalization and factorization scales fixed to a common value (the mass of top-quark).

Finally, for completeness the distributions for b-jet kinematics are given in Figure 6. Namely, the distribution in the transverse momentum p_{T_b} and the distribution in the rapidity y_b of the bottom quark are shown. Similarly to the bottom-anti-bottom pair kinematics, also here, small NLO corrections are visible. The shape of kinematic distributions can be distorted by 20% at most in some regions of phase space. This is once again contrary to the LHC case, where large and relatively constant NLO corrections have been obtained for

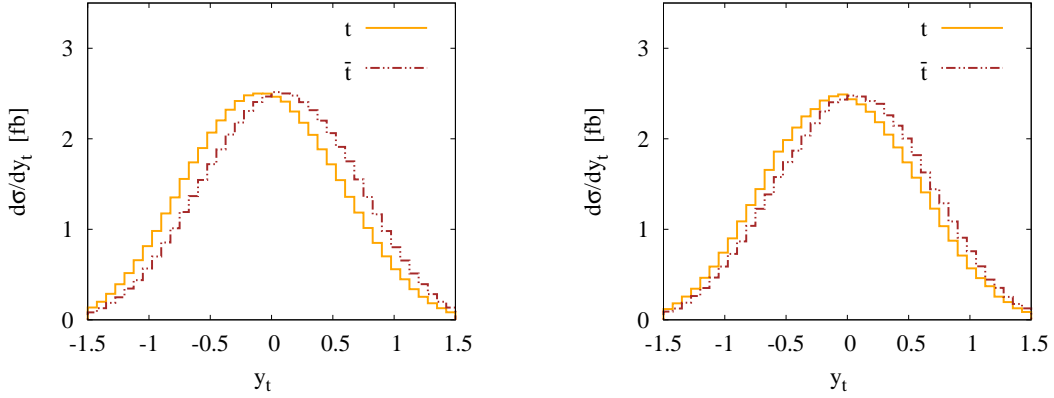


Figure 7. Differential cross section distributions as a function of rapidity, y_t , of the top and anti-top quark at LO (left panel) and NLO (right panel) for $p\bar{p} \rightarrow t\bar{t}b\bar{b} + X$ production at the TeVatron run II. The (orange) solid curve corresponds to the top quark, whereas the (brown) dash-dotted one to the anti-top quark.

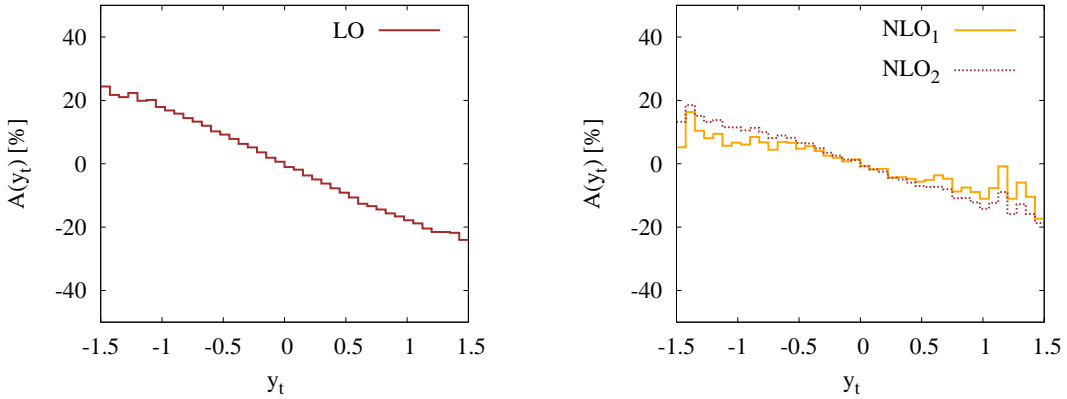


Figure 8. Differential asymmetry $A(t)$, as a function of the top quark rapidity at LO (left panel) and NLO (right panel) for $p\bar{p} \rightarrow t\bar{t}b\bar{b} + X$ production at the TeVatron run II. NLO_1 refers to a result with a consistent expansion in α_s , while NLO_2 to the unexpanded one.

$\mu = m_t$, whereas a dynamical scale and additional cuts allowed to reduce them down to 20% – 40%.

3.3 Forward-Backward Asymmetry

As a bonus of our study, we calculated the integrated top quark forward-backward asymmetry for the $t\bar{t}b\bar{b}$ production process at the TeVatron. At LO the asymmetry is defined

as

$$\mathcal{A}_{\text{FB,LO}}^t = \frac{\sigma_{\text{LO}}(y_t > 0) - \sigma_{\text{LO}}(y_t < 0)}{\sigma_{\text{LO}}(y_t > 0) + \sigma_{\text{LO}}(y_t < 0)}, \quad (3.7)$$

where y_t is the rapidity of the top quark and $\sigma_{\text{LO}}^\pm = \sigma_{\text{LO}}(y_t > 0) \pm \sigma_{\text{LO}}(y_t < 0)$ is evaluated with LO PDFs and LO α_s . On the other hand, the asymmetry at NLO is expressed through

$$\mathcal{A}_{\text{FB,NLO}}^t = \frac{\sigma_{\text{LO}}^- + \delta\sigma_{\text{NLO}}^-}{\sigma_{\text{LO}}^+ + \delta\sigma_{\text{NLO}}^+}, \quad (3.8)$$

where $\delta\sigma_{\text{NLO}}^\pm$ are the NLO contributions to the cross sections and σ_{LO}^\pm are evaluated this time with NLO PDFs and NLO α_s . The ratio generates contributions of $\mathcal{O}(\alpha_s^2)$ and higher, which are affected by unknown next-to-next-to-leading order contributions. Therefore, it is necessary to expand Equation (3.8) to first order in α_s . The following definition is then obtained [44, 45]

$$\mathcal{A}_{\text{FB,NLO}}^t = \frac{\sigma_{\text{LO}}^-}{\sigma_{\text{LO}}^+} \left(1 + \frac{\delta\sigma_{\text{NLO}}^-}{\sigma_{\text{LO}}^-} - \frac{\delta\sigma_{\text{NLO}}^+}{\sigma_{\text{LO}}^+} \right). \quad (3.9)$$

The integrated forward-backward asymmetry of the top quark at LO for $t\bar{t}b\bar{b}$ production amounts to (the error in parentheses corresponds to scale variation)

$$\mathcal{A}_{\text{FB,LO}}^t = -0.088(2). \quad (3.10)$$

With NLO corrections, the asymmetry is reduced down to

$$\mathcal{A}_{\text{FB,NLO}}^t = -0.044(6), \quad (3.11)$$

when a definition with a consistent expansion in α_s is used. For an unexpanded ratio of the NLO cross sections, the result is

$$\mathcal{A}_{\text{FB,NLO}}^t = -0.061(14). \quad (3.12)$$

The two NLO definitions give results which differ by about 40% for the central scale. Also the theoretical error as calculated from the scale dependence is more than a factor 2 higher in the latter case.

In Figure 7, the rapidity distributions for the top and anti-top quarks are presented at LO and NLO. Results are not symmetric around $y_t = 0$ and are shifted to a forward direction for the anti-top quarks and a backward direction for the top quarks. This shows that anti-top quarks are preferentially emitted in the direction of the incoming protons.

In Figure 8, we have also plotted the differential asymmetry, $\mathcal{A}(y_t)$. It rises up to $\pm 20\%$ at LO and well above $\pm 10\%$ at NLO in suitably chosen kinematical regions. After including the NLO corrections the forward-backward asymmetry of top quarks is reduced by a factor 2 as can be seen both from Equation (3.10) and Equation (3.11) as well as in Figure 8.

4 Summary and Conclusions

In this paper, a computation of the NLO QCD corrections to the top quark pair production in association with two hard b-jets at the TeVatron run II has been presented. The total cross section and its scale dependence, together with a few differential distributions have been given. The impact of the NLO QCD corrections on the integrated cross sections as calculated for the fixed scale $\mu_F = \mu_R = \mu = m_t$, is small, of the order of 2%. Moreover, the NLO QCD corrections reduce the scale uncertainty of the total cross sections as compared to LO calculations. As a further matter, the NLO corrections to the differential distributions are below 10% in the phenomenologically significant regions, reaching 20% at some corners of the phase space.

Since at the TeVatron, the corrections are small, the integrated and differential \mathcal{K} -factors do not necessarily need to be applied in the background estimation for the $t\bar{t}H \rightarrow t\bar{t}b\bar{b}$ signal process at the TeVatron. At least not for the observables which have been scrutinized here. Definitely, an application of the large LHC \mathcal{K} -factor to TeVatron phenomenological analyzes dramatically overestimates the size of the irreducible $t\bar{t}b\bar{b}$ background.

Let us conclude by noting that the predicted rates are very small. Combined with the luminosity of the TeVatron they amount to just a few events. The relevance of the present study lies, however, in the fact that Higgs exclusion bounds are obtained using a combination of data from different production channels with the $t\bar{t}H$ process, and thus its irreducible background, also taken into account by the CDF and D0 collaborations.

Acknowledgments

The calculations have been performed on the Grid Cluster of the Bergische Universität Wuppertal, financed by the Helmholtz - Alliance Physics at the Terascale and the BMBF. The author was supported by the Initiative and Networking Fund of the Helmholtz Association, contract HA-101 (Physics at the Terascale).

The author would like to thank Christian Schwanenberger for motivating her to perform this study.

References

- [1] W. Beenakker, S. Dittmaier, M. Kramer, B. Plumper, M. Spira and P. M. Zerwas, *Higgs radiation off top quarks at the Tevatron and the LHC*, Phys. Rev. Lett. **87** (2001) 201805, [[hep-ph/0107081](#)].
- [2] L. Reina and S. Dawson, *Next-to-leading order results for t anti- t h production at the Tevatron*, Phys. Rev. Lett. **87** (2001) 201804, [[hep-ph/0107101](#)].
- [3] L. Reina, S. Dawson and D. Wackerth, *QCD corrections to associated t anti- t h production at the Tevatron*, Phys. Rev. D **65** (2002) 053017, [[hep-ph/0109066](#)].
- [4] W. Beenakker, S. Dittmaier, M. Kramer, B. Plumper, M. Spira and P. M. Zerwas, *NLO QCD corrections to t anti- t H production in hadron collisions*, Nucl. Phys. B **653** (2003) 151, [[hep-ph/0211352](#)].

- [5] CDF and D0 Collaborations, *Combined CDF and D0 Upper Limits on Standard Model Higgs Boson Production with up to 8.6 fb^{-1} of Data*, arXiv:1107.5518 [hep-ex].
- [6] D0 Collaboration, *Search for the Standard Model Higgs boson in the $t\bar{t}H \rightarrow t\bar{t}b\bar{b}$ channel*, D0 note 5739-CO NF, (2009).
- [7] CDF Collaboration, *Search for SM Higgs boson production in association with $t\bar{t}$ using no lepton final state*, CDF note 10582, (2011).
- [8] G. Bevilacqua, M. Czakon, C. G. Papadopoulos, R. Pittau and M. Worek, *Assault on the NLO Wishlist: $pp \rightarrow t\bar{t}b\bar{b}$* , JHEP **0909** (2009) 109, [arXiv:0907.4723 [hep-ph]].
- [9] G. Bevilacqua, M. Czakon, C. G. Papadopoulos and M. Worek, *Dominant QCD Backgrounds in Higgs Boson Analyses at the LHC: A Study of $pp \rightarrow t$ anti- $t + 2$ jets at Next-To-Leading Order*, Phys. Rev. Lett. **104** (2010) 162002, [arXiv:1002.4009 [hep-ph]].
- [10] G. Bevilacqua, M. Czakon, C. G. Papadopoulos and M. Worek, *Hadronic top-quark pair production in association with two jets at Next-to-Leading Order QCD*, arXiv:1108.2851 [hep-ph].
- [11] G. Bevilacqua, M. Czakon, A. van Hameren, C. G. Papadopoulos and M. Worek, *Complete off-shell effects in top quark pair hadroproduction with leptonic decay at next-to-leading order*, JHEP **1102** (2011) 083, [arXiv:1012.4230 [hep-ph]].
- [12] A. Bredenstein, A. Denner, S. Dittmaier and S. Pozzorini, *NLO QCD corrections to $pp \rightarrow t$ anti- $t b$ anti- $b + X$ at the LHC*, Phys. Rev. Lett. **103** (2009) 012002, [arXiv:0905.0110 [hep-ph]].
- [13] A. Bredenstein, A. Denner, S. Dittmaier and S. Pozzorini, *NLO QCD Corrections to Top Anti-Top Bottom Anti-Bottom Production at the LHC: 2. full hadronic results*, JHEP **1003** (2010) 021, [arXiv:1001.4006 [hep-ph]].
- [14] A. Denner, S. Dittmaier, S. Kallweit and S. Pozzorini, *NLO QCD corrections to $WWbb$ production at hadron colliders*, Phys. Rev. Lett. **106** (2011) 052001, [arXiv:1012.3975 [hep-ph]].
- [15] G. Ossola, C. G. Papadopoulos and R. Pittau, *Reducing full one-loop amplitudes to scalar integrals at the integrand level*, Nucl. Phys. B **763** (2007) 147, [hep-ph/0609007].
- [16] G. Bevilacqua, M. Czakon, M. V. Garzelli, A. van Hameren, A. Kardos, C. G. Papadopoulos, R. Pittau and M. Worek, *Helac-nlo*, arXiv:1110.1499 [hep-ph].
- [17] G. Ossola, C. G. Papadopoulos and R. Pittau, *CutTools: A Program implementing the OPP reduction method to compute one-loop amplitudes*, JHEP **0803** (2008) 042, [arXiv:0711.3596 [hep-ph]].
- [18] G. Ossola, C. G. Papadopoulos and R. Pittau, *On the Rational Terms of the one-loop amplitudes*, JHEP **0805** (2008) 004, [arXiv:0802.1876 [hep-ph]].
- [19] P. Mastrolia, G. Ossola, C. G. Papadopoulos and R. Pittau, *Optimizing the Reduction of One-Loop Amplitudes*, JHEP **0806** (2008) 030, [arXiv:0803.3964 [hep-ph]].
- [20] P. Draggiotis, M. V. Garzelli, C. G. Papadopoulos and R. Pittau, *Feynman Rules for the Rational Part of the QCD 1-loop amplitudes*, JHEP **0904** (2009) 072, [arXiv:0903.0356 [hep-ph]].
- [21] A. van Hameren, C. G. Papadopoulos and R. Pittau, *Automated one-loop calculations: A Proof of concept*, JHEP **0909** (2009) 106, [arXiv:0903.4665 [hep-ph]].

- [22] M. Czakon, C. G. Papadopoulos and M. Worek, *Polarizing the Dipoles*, JHEP **0908** (2009) 085, [[arXiv:0905.0883 \[hep-ph\]](#)].
- [23] A. van Hameren, *Kaleu: a general-purpose parton-level phase space generator*, [arXiv:1003.4953 \[hep-ph\]](#).
- [24] C. G. Papadopoulos, *PHEGAS: A Phase space generator for automatic cross-section computation*, Comput. Phys. Commun. **137** (2001) 247, [[hep-ph/0007335](#)].
- [25] A. van Hameren, *OneLOop: For the evaluation of one-loop scalar functions*, Comput. Phys. Commun. **182** (2011) 2427, [[arXiv:1007.4716 \[hep-ph\]](#)].
- [26] A. Kanaki and C. G. Papadopoulos, *HELAC: A Package to compute electroweak helicity amplitudes*, Comput. Phys. Commun. **132** (2000) 306, [[hep-ph/0002082](#)].
- [27] C. G. Papadopoulos and M. Worek, *Multi-parton cross sections at hadron colliders*, Eur. Phys. J. C **50** (2007) 843, [[hep-ph/0512150](#)].
- [28] A. Cafarella, C. G. Papadopoulos and M. Worek, *Helac-Phegas: A Generator for all parton level processes*, Comput. Phys. Commun. **180** (2009) 1941, [[arXiv:0710.2427 \[hep-ph\]](#)].
- [29] T. Gleisberg, F. Krauss, C. G. Papadopoulos, A. Schaelicke and S. Schumann, *Cross-sections for multiparticle final states at a linear collider*, Eur. Phys. J. C **34** (2004) 173, [[hep-ph/0311273](#)].
- [30] J. Alwall, S. Hoche, F. Krauss, N. Lavesson, L. Lonnblad, F. Maltoni, M. L. Mangano and M. Moretti *et al.*, *Comparative study of various algorithms for the merging of parton showers and matrix elements in hadronic collisions*, Eur. Phys. J. C **53** (2008) 473, [[arXiv:0706.2569 \[hep-ph\]](#)].
- [31] C. Englert, B. Jager, M. Worek and D. Zeppenfeld, *Observing Strongly Interacting Vector Boson Systems at the CERN Large Hadron Collider*, Phys. Rev. D **80** (2009) 035027, [[arXiv:0810.4861 \[hep-ph\]](#)].
- [32] S. Actis *et al.* [Working Group on Radiative Corrections and Monte Carlo Generators for Low Energies Collaboration], *Quest for precision in hadronic crosssections at low energy: Monte Carlo tools vs. experimental data*, Eur. Phys. J. C **66** (2010) 585, [[arXiv:0912.0749 \[hep-ph\]](#)].
- [33] C. Carloni Calame, H. Czyz, J. Gluza, M. Gunia, G. Montagna, O. Nicrosini, F. Piccinini and T. Riemann *et al.*, *NNLO leptonic and hadronic corrections to Bhabha scattering and luminosity monitoring at meson factories*, JHEP **1107** (2011) 126, [[arXiv:1106.3178 \[hep-ph\]](#)].
- [34] CDF and D0 Collaborations, *Combination of CDF and D0 Results on the Mass of the Top Quark Using Up to 5.6 fb⁻¹ of Data*, [arXiv:1007.3178 \[hep-ex\]](#).
- [35] A. D. Martin, W. J. Stirling, R. S. Thorne and G. Watt, *Parton distributions for the LHC*, Eur. Phys. J. C **63** (2009) 189, [[arXiv:0901.0002 \[hep-ph\]](#)].
- [36] S. Catani, Y. L. Dokshitzer and B. R. Webber, *The K_⊥ perpendicular clustering algorithm for jets in deep inelastic scattering and hadron collisions*, Phys. Lett. B **285** (1992) 291.
- [37] S. Catani, Y. L. Dokshitzer, M. H. Seymour and B. R. Webber, *Longitudinally invariant K_t clustering algorithms for hadron hadron collisions*, Nucl. Phys. B **406** (1993) 187.
- [38] S. D. Ellis and D. E. Soper, *Successive combination jet algorithm for hadron collisions*, Phys. Rev. D **48** (1993) 3160 [[hep-ph/9305266](#)].

- [39] M. Cacciari, G. P. Salam and G. Soyez, *The Anti- $k(t)$ jet clustering algorithm*, JHEP **0804** (2008) 063, [[arXiv:0802.1189 \[hep-ph\]](#)].
- [40] Y. L. Dokshitzer, G. D. Leder, S. Moretti and B. R. Webber, *Better jet clustering algorithms*, JHEP **9708** (1997) 001, [[hep-ph/9707323](#)].
- [41] Z. Nagy and Z. Trocsanyi, *Next-to-leading order calculation of four jet observables in electron positron annihilation*, Phys. Rev. D **59** (1999) 014020, [Erratum-ibid. D **62** (2000) 099902], [[hep-ph/9806317](#)].
- [42] S. Catani and M. H. Seymour, *A General algorithm for calculating jet cross-sections in NLO QCD*, Nucl. Phys. B **485** (1997) 291, [Erratum-ibid. B **510** (1998) 503], [[hep-ph/9605323](#)].
- [43] S. Catani, S. Dittmaier, M. H. Seymour and Z. Trocsanyi, *The Dipole formalism for next-to-leading order QCD calculations with massive partons*, Nucl. Phys. B **627** (2002) 189, [[hep-ph/0201036](#)].
- [44] S. Dittmaier, P. Uwer and S. Weinzierl, *NLO QCD corrections to t anti- t + jet production at hadron colliders*, Phys. Rev. Lett. **98** (2007) 262002, [[hep-ph/0703120 \[hep-ph\]](#)].
- [45] S. Dittmaier, P. Uwer and S. Weinzierl, *Hadronic top-quark pair production in association with a hard jet at next-to-leading order QCD: Phenomenological studies for the Tevatron and the LHC*, Eur. Phys. J. C **59** (2009) 625, [[arXiv:0810.0452 \[hep-ph\]](#)].